Increased second harmonic output power using walk-off compensation in birefringent crystals

1991 J. Phys.: Condens. Matter 3 7421

(http://iopscience.iop.org/0953-8984/3/38/014)

J. Phys.: Condens. Matter 3 (1991) 7421–7433. Printed in the UK

Increased second harmonic output power using walk-off compensation in birefringent crystals

T Yanagawa†‡ and L K Samanta§

† Basic Research Laboratories, Nippon Telegraph and Telephone Corporation, Musashino-shi, Tokyo 180 Japan

Received 28 January 1991

Abstract. A new technique utilizing the double refraction walk-off of a precisely cut pair of KTP crystals and a mode-locked Nd:YAG laser to obtain efficient second harmonic generation (SHG) is reported for the first time. This technique leads to a fourfold increment in second harmonic output power compared with that of a single crystal and would open up a number of potential new applications.

1. Introduction

The second harmonic generation (SHG) of laser light is a well established technique capable of being carried out with a high degree of efficiency. Continuous work in the field of parametric interactions has resulted in optical amplifiers and oscillators that can be tuned over a range of an octave or more. SHG by mixing two strong collinear waves at a fundamental frequency often uses a technique which phase matches acentric crystals to increase efficiency and this same technique can also be used with acentric biaxial crystals. SHG with fundamental waves of the same polarization is termed type I, while that with orthogonal polarization is type II. An additional disadvantage of phase-matching at $\theta \neq 90°$, usually termed critical phase-matching (CPM), is that there is a walk-off of the electromagnetic wave from the polarization wave due to double refraction of waves with a finite aperture. However, phase-matching at $\theta = 90°$, termed non-critical phase-matching (NCPM), has obvious merit for device applications due to its additional advantage of having no such walk-off due to double refraction. Thus, if the refractive indices can be adjusted so as to achieve NCPM under a variety of parameters such as temperature, crystal chemical composition, non-collinearity, stress, etc, then the walk-off effect could be eliminated and the efficiency of various non-linear phase-matched interactions increased.

However, the stringent phase-matching conditions required for the non-linear processes do not permit the process to be adjusted to achieve NCPM. Therefore, walk-off due to double refraction has a deleterious effect on the efficiency. Energy conversion from the fundamental to the harmonic wave is a complicated function of propagation direction, polarization, index properties and sign as well as the magnitude of the

‡ Present address: NTT Opto-electronics Laboratories, 3-1, Morinosato Wakamiya, Atsugi-shi, Kanagawa Pref. 243-01 Japan.

§ Visiting scientist, Department of Physics, Burdwan University, Burdwan 713104, West Bengal, India.

0953-8984/91/387421+13$03.50

second-order polarizability tensor. This consideration makes it is very important to eliminate the effect of walk-off from the various non-linear interactions since walk-off compensation plays a key role in the study of such various current and attractive topics as quantum non-demolition measurement, squeezed states, etc. In this light, a detailed study of walk-off compensation has been made for the first time using a pair of biaxial crystals, in this case KTP [1]. The results are very encouraging with regard to future applications and are discussed in detail in this paper.

2. Crystal characteristics and properties

The compound potassium titanyl phosphate [2–5], commonly known as KTP (chemical formula $KTiOPO_4$), has emerged as being superior among the non-linear materials used for laser radiation conversion. With a high non-linear optical coefficient comparable with that of $Ba_2NaNb_5O_{15}$ (BNN), and a high optical strength, as well as being chemically inert with a high mechanical stability and free from induced optical inhomogeneity, KTP is characterized by broad spectra, temperature and angular bandwidths that make it the best choice for generating SH from Nd:YAG laser radiation. KTP also has the advantage that it can be phase-matched using either type I or II interactions. Furthermore, the crystal is transparent in the 350–4500 nm region and the superiority of the improved flux technique over the hydrothermal growth method results in the absence of the O–H absorption peak at 2800 nm which usually appears in the flux method.

The KTP crystal belongs to orthorhombic point group $mm2$ and usually corresponds to point group mmm, both of which are included in the space group $Pna2_1$, even though x-ray analysis indicates the presence of eight molecules per unit cell. The crystal structure of KTP is composed of alternating PO_4 tetrahedra and distorted TiO_6 octahedra with potassium ions situated in channels between them. The large non-linearity of this compound is thought to be due to the fact that the Ti–O bond is the shortest in the crystal.

3. Some aspects of second harmonic generation

Harmonic generation is now commonly used to extend the laser wavelength range down to the UV or XUV region and SHG is presently a standard technique [6–8] for generating tunable laser radiation in different parts of the electromagnetic spectrum depending on the materials and incident pump radiation used. In particular, the region around ~ 500 nm has aroused considerable technological interest because of its applications in under water communications. Garmash *et al* [9] reported SHG using a 1079.6 nm Nd:$YAlO_3$ laser (YALO), while blue light (459 nm) radiation was generated by Baumert *et al* [10] using NCPM interactions caused by sum-mixing 1064 and 809 nm with KTP and Kato [11] and Fan *et al* [12] have reported SHG of Nd:YAG lasers at 1064 nm. The most frequent SHG applications are to frequency double the output of Nd:YAG lasers to produce a green beam $\lambda = 532$ nm from $\lambda = 1064$ nm and to generate tunable UV radiation down to 210 nm by frequency doubling tunable dye lasers.

We have experimentally investigated type II phase-matching since it is attractive because of its large angular acceptance, bandwidth and high non-linear coefficient.

The theoretical analysis by Mehendale and Gupta [13] showed that reduced conversion efficiency due to walk-off occurs more in type II than type I phase-matching. Contrary to the idea of Boyd and Kleinman [14] which was to use arbitrary tight focusing with a limited parameter gain due to walk-off, Kuizenga [15] reported an increased parametric gain in a non-linear crystal with double refraction (walk-off) using elliptical beams since walk-off only occurred in the plane-of-propagation direction and the optic axis while full advantage could still be taken of tight focusing in the non-walk-off plane. Our experimental arrangement completely eliminated double refraction walk-off by utilizing a technique for doubling the crystal length (using a pair of crystals with the same length and a proper orientation) and, thus, we achieved almost four times the output power available from a single crystal.

Phase-matching allows enhanced SHG to be achieved and accomplished in anisotropic crystals by making birefringent equal dispersion at the commonly known phase-matching angle. However, SHG is limited by double refraction [16, 17] since it is known that the energy propagation direction or Poynting vector is given by the normal to the index surface for any phase propagation direction. The double refraction measurement is given by the angle ρ, which for a positive uniaxial crystal is given as

$$\rho \approx \tan\rho = \frac{1}{2}(n_\omega^e)^2 \left[\frac{1}{(n_{2\omega}^o)^2} - \frac{1}{(n_{2\omega}^e)^2}\right] \sin 2\theta_m. \tag{1}$$

For an ordinary wave both vectors are parallel, but for an extraordinary wave, the Poynting vector deviates from the phase propagation by the angle mentioned where the polarization in equation (1) is reversed for a negative crystal.

Double refraction causes harmonic separation (walk-off) from the fundamental wave for beams with a finite diameter and, thus, ultimately limits the effective volume over which the interaction takes place. For $\rho \neq 0$, the aperture length l_a is approximately a/ρ where a is the beam diameter. When $l_a \rightarrow \infty$ with $\rho = 0$, the SHG increases, but it is limited by the diffraction effect instead of the aperture length. Two additional problems are that the double refraction effect is more pronounced the longer the sample is and that the spot size is smaller. Even though the phase-matching characteristics of the crystals limit the use of crystals for a no walk-off condition, they can be eliminated by NCPM, also known as 90° phase-matching, with additional advantages in the acceptance angle and effective non-linear coefficient over CPM. This has been achieved in $LiNbO_3$ by temperature tuning, but the disadvantage of temperature tuning [18] is that the crystal temperature often has to be held within a strict tolerance limit to maintain phase-matching.

The SHG of an in-focus laser beam has been analysed, but Boyd and Kleinman [14] pointed out that the criteria for optimum interaction using a collinear focused beam occur when both beams have the same focus and confocal parameter rather than the same spot size. If the effects of beam divergence on focusing and the Boyd and Kleinman focusing factor $h(B,\xi)$ are included, SHG efficiency can be defined as [19]

$$\eta = \frac{P_{2\omega}}{P_\omega} = \left(\frac{2\omega^2 d_{\text{eff}}^2}{\pi n_\omega^2 n_{2\omega} \epsilon_0 c^3}\right) P_\omega l k_\omega h(B,\xi) \tag{2}$$

where the double refraction parameter $B = \frac{1}{2}\rho(lk_\omega)^{1/2}$, the focusing parameter $\xi = l/b$, and b is the confocal parameter. For a small walk-off angle which means small B,

that is for a crystal length which is shorter than the aperture length, $h(B,\xi) \rightarrow \bar{h}(B,\xi)$ and in the near-field approximation with negligible double refraction $\bar{h}(B,\xi) \rightarrow \xi$.

Since the gain is limited by double refraction, the introduction of a useful crystal length $l_{\text{eff}}(l)$ is very important, $l_{\text{eff}} \approx \lambda_0/2n_\omega\rho^2$. Under a strong double refraction limit such as $l_{\text{eff}} \ll l$, the gain reduction factor $\bar{h}_m(B,\xi) \rightarrow \pi/4B^2$ and l in equation (2) should be replaced by l_{eff}. Thus, if $\rho \neq 0$, the aperture limits the interaction so that even a small walk-off angle will reduce the SH efficiency by as much as 30 times for a given crystal length and focusing in turn necessitates adjustment of the crystal refractive indices to achieve NCPM if it is possible according to the phase-matching condition.

Therefore, attaining NCPM to avoid double refraction is not an easy task. However, Ashkin *et al* [20] reported phase-matched SHG without double refraction using a KDP waveguide structure. This is possible due to the availability of large size KDP crystals because of the improved crystal growth technology for this type of crystal only. The same technology cannot be used for the established non-linear crystals [21] because of size, shape and quality and the more important point that it is not possible to obtain SH power, which was observed in our experimental arrangement.

4. Experimental details and results

This article reports an experimental arrangement, shown in figure 1(*a*), to obtain sufficient SH power using a pair of KTP crystals that is possible with existing methods. A mode-locked Nd:YAG laser is used to pump KTP crystals for SH generation of 532 nm with an average fundamental input power of 4.7 W and a pulsewidth of about 90 ps. Two KTP crystals cut from the same piece of a well grown crystal (as per our requirement) to a size of 5 mm × 5 mm × 5 mm and oriented for type II interaction at 1064 nm were used. Although the refractive indices allow the use of both type I and II for SHG, d_{eff} is too small to permit type I phase-matching; therefore, type II was automatically preferred.

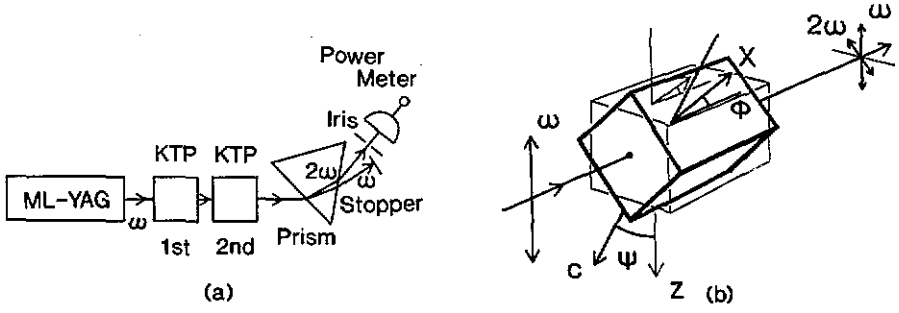

Figure 1. (*a*) Experimental setup for measurement of SH (2ω) output power. Mode-locked Nd:YAG laser and a pair of KTP crystals are used to generate a 2ω wave. The fundamental (ω) and 2ω waves are separated by an SF6 prism. (*b*) The phase-matching condition ($\theta = 90°$, $\phi \approx 22°$) of the KTP crystal. SH output power is measured as a function of ψ.

The type II phase-matching condition in a KTP crystal is shown in figure 1(*b*). The laser beam is set normal to the z-direction and c-axis indicating $\theta = 90°$ is cut in the

XY-plane at angle ϕ from the X-direction, where ϕ is the phase-matching angle (i.e. $\phi \approx 22°$ in this case). When the polarization direction of the fundamental YAG laser (1064 nm) is vertical, the c-axis of the crystal should be tilted 45° from the Z-axis and the polarization direction of the laser beam to obtain the maximum SH output power. The two KTP crystals used in this arrangement are labelled first and second in the laser positioning shown in figure 1(a).

At the beginning of the experiment one KTP crystal is positioned and adjusted to obtain the maximum SH power in the phase-matching direction. The optimum polarization direction of the pumping beam can be obtained by rotating the crystal around the beam propagation direction and is defined as $\psi = 0$, where ψ is the angle between the c-axis and the reference direction defined as optimum. This result is shown in figure 2 as a function of ψ. The SH output at 532 nm is separated from the 1064 nm fundamental wave by the SF6 prism shown in figure 1(a) and the average power was measured with a coherent 212 power meter with a Si head. It becomes clear that the SH output has four peaks.

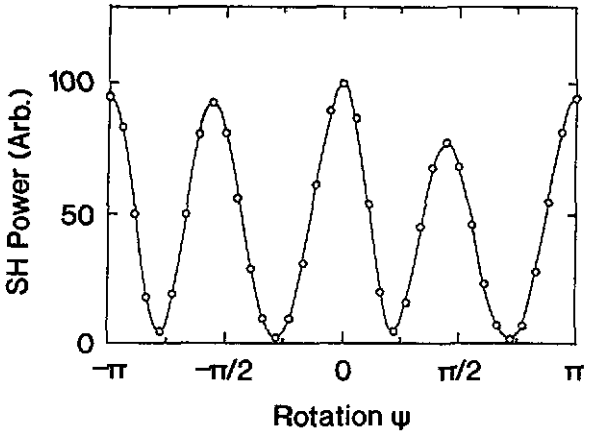

Figure 2. SH output power of one KTP crystal as a function of rotation angle ψ as shown in figure 1(b).

The result can be analysed with second-order polarizability tensor d_{ij} of the KTP and direction cosines [22]. The relationships between angles θ, ϕ and δ are illustrated in figure 3. Angles θ and ϕ have already been described. δ is the angle between one polarization direction, e_1, of the fundamental wave and ZH, where ZH is a vector tangential to the fundamental propagation direction at a given point H. Polarization vectors e_1 and e_2 are the two components of the fundamental wave and are perpendicular to each other. These amplitudes are defined as $E_\omega^{e_1}$ and $E_\omega^{e_2}$ using the function of crystal rotation ψ. The amplitude of the input electric field is defined as E_ω. Therefore, the SH power realized from the second-order non-linear polarizability in the XY-plane is

$$|P_{2\omega}|^2 = \frac{A^2}{8}\{1 + \cos(4\psi)\} \tag{3}$$

where

$$A \equiv (d_{15}\sin^2\phi + d_{24}\cos^2\phi)\sin\theta E_\omega^2. \tag{4}$$

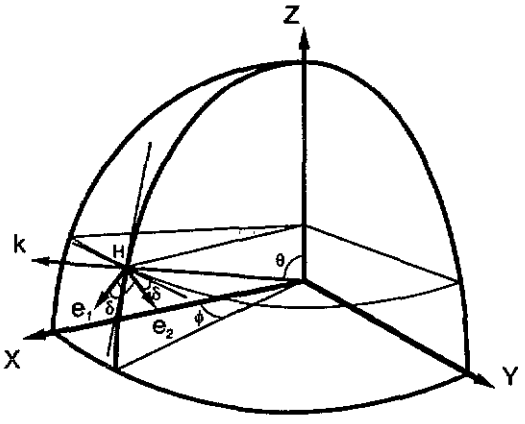

Figure 3. The relationship of the propagation direction k, polarization directions e_1 and e_2, and coordinates (X, Y and Z) represented by angles θ, ϕ and δ.

This equation is derived in the appendix and easily explains the SHG of the KTP crystal shown in figure 2.

The SH power from a pair of crystals has also been measured. To begin with, when the second crystal is adjusted to obtain the maximum SH power, the first crystal placed in front of the laser beam should obtain maximum total power near the phase-matching condition. Then, the first crystal is rotated while the second crystal remains fixed. Measurement of the SH power with a pair of crystals with properly oriented c-axes shows a unique solution for obtaining maximum power. Even more interesting is that this is observed at only one particular orientation of the two crystals in which *complete walk-off compensation* takes place, thus yielding an extremely high SH output power almost four times larger than that obtained with a single crystal [1], as shown in figure 4. Moreover, SH output power was also observed when the input facet was turned to output in the second crystal. This is shown in figure 5(b) along with the results taken before turning shown in figure 5(a). It seems that the value of ψ giving *maximum SH output power in (a) shifts by 180° from that in (b)*, which will be discussed later. This difference may originate from a difference in crystal orientation, as shown in figures 6(a) and (b).

SH output enhanced by walk-off compensation resulting from the same arrangement as figure 4 is shown in figure 6(a), and it is suppressed by the configuration shown in figure 6(b). *The electric field of the ordinary wave is conserved in (a); however,* the signs for the X and Y elements in the wave's field are different for each crystal and suppress each other in (b).

With similar treatment in the one crystal case, the SH power as a function of the rotation angle of the first crystal can be simply analysed as described in the appendix. If pump depression is assumed not to exist, the SH electric fields of each crystal can be simply superposed, and the first crystal's SH electric field component of the second crystal's XY-plane combined with the second crystal's SH field. The combined SH field of the XY-plane and the first crystal's on the second crystal's Z-axis can then provide the total SH power. As a result, the normalized total SH power of the configurations

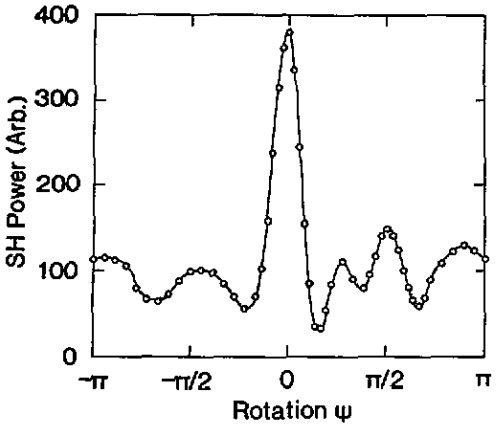

Figure 4. SH output power of KTP crystal pair as a function of rotation angle ψ of the first crystal. The walk-off compensation condition is realized at $\psi = 0$ which corresponds to the arrangement in which the c-axes of the two crystals are opposite to each other.

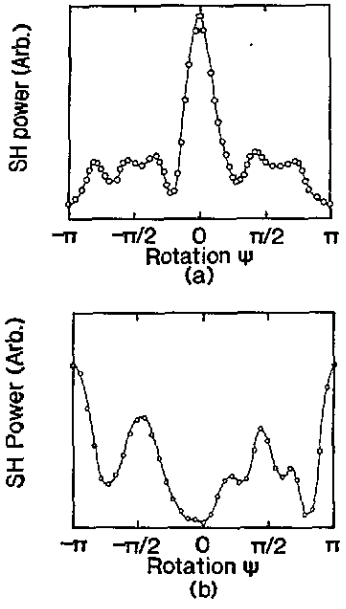

Figure 5. SH output power difference due to facet replacement of the second crystal as a function of the rotation angle ψ of the first crystal: (a) around the walk-off compensation condition; (b) the other arrangement of the second crystal facet replacement to opposite side.

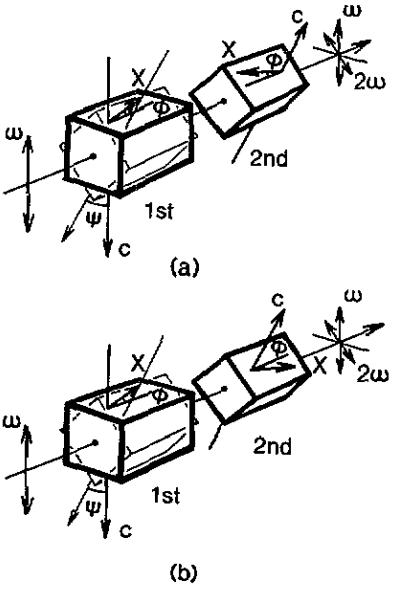

Figure 6. Crystal displacement figure. Arrangements (a) and (b) correspond to figure 5(a) and (b), respectively.

shown in figure 6(a) and (b) can be written as

$$|P_{2\omega}^{\text{total}}|^2 = \frac{A^2}{8}\{\cos(4\psi) \pm \cos(3\psi) \pm \cos\psi + 3\}. \tag{5}$$

The signs of the terms $\cos(3\psi)$ and $\cos\psi$ correspond to figure 5(a) and (b), that is (a) is positive and (b) is negative. The results of equation (5) are shown in figures 7(a) and (b). It is true that these analytical processes do not include the walk-off effect; however, the characteristic tendency of the total power to be dependent on the rotation angle of the first crystal can clearly be seen. Whether or not walk-off compensation takes place is conveniently confirmed by the SH output power at its maximum point. The experimental results can be said to be in good agreement with the analytical ones at this viewpoint.

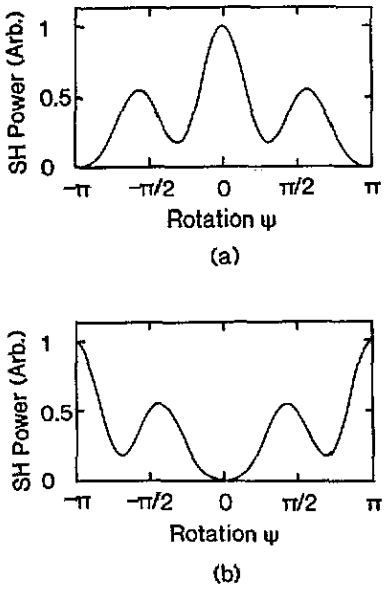

Figure 7. The analytical results of normalized SH output power: (a) the around walk-off compensation condition corresponds to figures 5(a) and 6(a). (b) The other corresponds to figures 5(b) and 6(b).

It should be noted that the differences in detail between figures 4 and 5(a) seems to be caused by reflection and scattering changes due to subtle optical path changes. This occurs, as the crystal facets are not anti-reflection-coated in this experiment and the crystals include points with slight local damage.

5. Discussions and conclusion

Since the useful crystal length is limited by the Poynting vector walk-off (aperture effect) and group velocity differences result in reduced efficiency in harmonic generation, a large difference between the fundamental wave and the SH is significant. Our results on enhanced SH output power clearly point out that walk-off compensation can be achieved with two properly cut crystal orientations. Non-collinear matching between an e-ray and o-ray in which the angle between the two input wavevectors inside the crystal is made just equal but opposite in magnitude to the walk-off of the e-ray could be utilized to obtain enhanced output power as there is a complete overlap of the input beams throughout the entire crystal. However, this is often uncertain due

to the phase-matching characteristics of the crystals. Although various approaches to increase the SH output power have been tried, it was not possible to achieve this target experimentally using a single crystal. A longer crystal may increase power, but it is limited by double refraction walk-off. However, when one crystal length is cut into two pieces of equal length and properly aligned a considerable increase in output power results while eliminating the deleterious effect of the double refraction walk-off inherent to any phase-matched non-linear interactions (except 90° phase-matching). It is interesting to note in this connection that the value of d_{eff} (1.1×10^{-8} esu) of one KTP crystal obtained from the relation

$$d_{\text{eff}}^2 = \frac{1}{2}\left(\frac{\epsilon_0}{\mu_0}\right)^{3/2} P_{2\omega} \frac{n_\omega^2 n_{2\omega}}{\omega^2 l^2} \left[\frac{\sin^2(\Delta k l/2)}{(kl/2)^2}\right]^{-1} \frac{A}{P_\omega^2} \tag{6}$$

using our measured data, which are 4.7 W fundamental average input and 3 mW SH average output power, agrees well with other reported values. It should also be noted in this connection that the SH pulsewidth is about 0.7 times that of the fundamental one and the beam diameter is around 900 μm, while the SF6 prism loss, including reflections, was experimentally found to be about 30%.

Compared with other well established non-linear crystals such as BBO, KTP would be a more suitable non-linear crystal for femtosecond difference frequency generation (DFG) because of its larger d_{eff} and the elimination of double refraction, although the same can be applied to all phase-matched non-linear interactions. Thus, the technique we are proposing reflects an inherent nature towards overcoming the long-standing problem of double refraction walk-off in phase-matched non-linear interactions in anisotropic crystals and should have far-reaching consequences, not only for the progress of non-linear optics, but also for that of quantum optics, which includes quantum non-demolition measurements [23, 24] (QND) using SHG, parametric down conversion [25] and the generation of squeezed states [26]. Therefore, this technique should emerge as very important and useful in years to come.

Acknowledgments

One of the authors (Dr L K Samanta) would like to gratefully acknowledge NTT Japan for supporting him in his Visiting Scientist position. Both of the authors would further like to thank Dr Y Yamamoto for his support of this work and Mr Y Okamura for his assistance during the experiment.

Appendix

If light propagates in the k direction (θ, ϕ) with the e_1 and e_2 polarizations shown in figure 3, the arbitrary electric field can be written as

$$E_\omega = E_\omega^{e_1} e_1 + E_\omega^{e_2} e_2 \tag{A1}$$

where $E_\omega^{e_1}$ and $E_\omega^{e_2}$ are electric field components in the e_1 and e_2 directions, respectively. The e_1 and e_2 polarized waves have electric field components $(E_\omega^{e_1})_j$ and $(E_\omega^{e_2})_j$

(j =1, 2, 3) in rectangular coordinates and are given by the direction cosines $(a_j^{e_1})$ and $(a_j^{e_2})$,

$$(E_\omega^{e_1})_j = (a_j^{e_1})E_\omega^{e_1} \tag{A2}$$

$$(E_\omega^{e_2})_j = (a_j^{e_2})E_\omega^{e_2} \tag{A3}$$

where the direction cosines $(a_j^{e_1})$ and $(a_j^{e_2})$ are expressed by

$$(a_j^{e_1}) = \begin{pmatrix} \cos\theta\cos\phi\cos\delta - \sin\phi\sin\delta \\ \cos\theta\sin\phi\cos\delta + \cos\phi\sin\delta \\ -\sin\theta\cos\delta \end{pmatrix} \tag{A4}$$

$$(a_j^{e_2}) = \begin{pmatrix} -\cos\theta\cos\phi\sin\delta - \sin\phi\cos\delta \\ -\cos\theta\sin\phi\sin\delta + \cos\phi\cos\delta \\ \sin\theta\sin\delta \end{pmatrix}. \tag{A5}$$

Second-harmonic (SH) polarization $P_{2\omega}$ induced by the E_j and E_k electric fields in biaxial crystals was reported by Ito *et al* [22] and is represented by

$$(P_{2\omega})_i = d_{ijk}E_jE_k \tag{A6}$$

where d_{ijk} is the tensor element of second-order polarizability and i, j and k correspond to the X, Y and Z coordinates. When SH polarization $(P_{2\omega})_j$ radiates as the e_2 wave,

$$P_{2\omega}^{e_2} = a_i^{e_2}(P_{2\omega})_i \tag{A7}$$

therefore, SH polarization $P_{2\omega}^{e_2}$ of the type II phase-matching condition is

$$P_{2\omega}^{e_2} = a_i^{e_2}d_{ijk}a_j^{e_1}a_k^{e_2}E_\omega^{e_1}E_\omega^{e_2}. \tag{A8}$$

d_{ijk} can be rewritten with Kleinman's symmetry as $d_{ij}(j = 1, 2, \ldots, 6)$, because interchanging $E_\omega^{e_1}$ and $E_\omega^{e_2}$ causes no significant change in the physics. The d_{ij} of the KTP crystal (m-monoclinic) are given by

$$d_{ij} = \begin{pmatrix} 0 & 0 & 0 & 0 & d_{15} & 0 \\ 0 & 0 & 0 & d_{24} & 0 & 0 \\ d_{31} & d_{32} & d_{33} & 0 & 0 & 0 \end{pmatrix}. \tag{A9}$$

Thus

$$\begin{aligned} P_{2\omega}^{e_2} = \{&(d_{24} - d_{15})(3\cos^2\delta - 1)\sin\theta\cos\theta\sin^2\phi\sin\delta \\ &- 3(d_{31}\cos^2\phi + d_{32}\sin^2\phi)\sin\theta\cos^2\theta\sin^2\delta\cos\delta \\ &- (d_{31}\sin^2\phi + d_{32}\cos^2\phi)\sin\theta\cos\delta(3\cos^2\delta - 2) \\ &- d_{33}\sin^3\theta\sin^2\delta\cos\delta\}E_\omega^{e_1}E_\omega^{e_2} \\ \equiv\ & d_{\text{eff}}(\theta,\phi)E_\omega^{e_1}E_\omega^{e_2}. \end{aligned} \tag{A10}$$

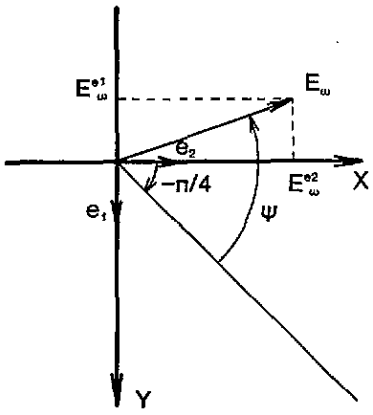

Figure A1. Polarization rotation ψ around propagation the k-axis. $E_\omega^{e_1}$ and $E_\omega^{e_2}$ are vector components of electric fields E_ω to e_1 and e_2 directions correspond to coordinates Y and X. Each component is perpendicular to the other.

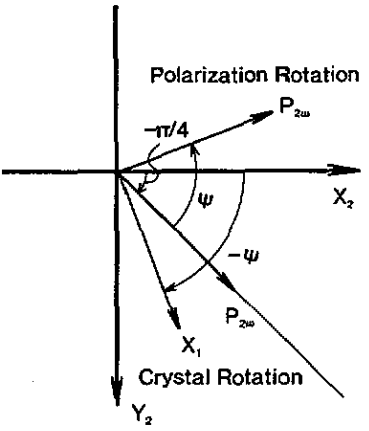

Figure A2. Polarization and crystal rotation around the propagation axis. Polarization rotation ψ corresponds to reverse crystal rotation $-\psi$, which is shown as the change to the first crystal X_1-axis from the second (X_2).

On the other hand, our experiments only studied SH as the o-wave. When SH polarization is defined as the e_2 direction at $\delta = 0$, the direction cosines $a_i^{e_2}, a_j^{e_1}$ are described by

$$(a_i^{e_2}) = \begin{pmatrix} -\sin\phi \\ \cos\phi \\ 0 \end{pmatrix} \tag{A11}$$

$$(a_j^{e_1}) = \begin{pmatrix} \cos\theta\cos\phi \\ \cos\theta\sin\phi \\ -\sin\theta \end{pmatrix}. \tag{A12}$$

The polarization rotation is represented as ψ, where ψ is defined as the angle from the line shown in figure A1, rotated $-\pi/4$ from the e_2 direction at $\delta = 0$. In this case, the electric field components are defined by

$$E_\omega^{e_1} = -E_\omega \sin(\psi - \pi/4) \tag{A13}$$

$$E_\omega^{e_2} = E_\omega \cos(\psi - \pi/4) \tag{A14}$$

then

$$P_{2\omega} = -\frac{A}{2}\cos(2\psi) \tag{A15}$$

$$A \equiv (d_{15}\sin^2\phi + d_{24}\cos^2\phi)E_\omega^2 \sin\theta \tag{A16}$$

where E_ω is the amplitude of the input electric field. At the conclusion of each crystal case, SH power at the power meter can be estimated by equation (A15) and rewritten as

$$|P_{2\omega}|^2 = \frac{A^2}{8}\{1 + \cos(4\psi)\}. \tag{A17}$$

The polarization rotation ψ is equal to the reverse rotation of the crystal around the k direction shown in figure A2. Then, crystal rotation $-\psi$ gives the same $P_{2\omega}$; however, the direction of $P_{2\omega}$ rotates with the crystal. When $\psi = \pi$, $P_{2\omega} = -A/2$ is the same as the value for $\psi = 0$, although it is produced in the opposite polarization space. Suppose that the SH polarization radiated from the first crystal exists at coordinates X_2 and Y_2 of the second crystal. In figure 6(b), the difference between the two crystals is only in the direction of the c-axis. Therefore, the polarization components $(P_{2\omega})_{X_2}$ and $(P_{2\omega})_{Y_2}$ at the X_2 and Y_2 coordinates of the second crystal are represented by $P_{2\omega}$ multiplied by $\cos(-\psi)$ and $\sin(-\psi)$, respectively. According to the discussion earlier, $P_{2\omega}$ in the X_2 direction at $\psi = \pi$ becomes $A/2$ and the total SH power $|P_{2\omega}^{\text{total}}|^2$ behind the second crystal becomes

$$|P_{2\omega}^{\text{total}}|^2 = \frac{A^2}{8}\{\cos(4\psi) - 2\cos(3\psi) - 2\cos\psi + 3\} \tag{A18}$$

where $\psi = 0$ represents the c-axis of the first crystal opposite to that of the second crystal in figure 6(b) which gives $|P_{2\omega}^{\text{total}}|^2 = 0$.

In the case of figure 6(a), the second crystal is rotated by π around the Z-axis from the position of the first crystal; therefore, the rotation tensor of the coordinate is needed. Suppose that rotation ξ of the Z-axis is defined as $R_Z(\xi)$ and the π rotation of the k-axis is R_k; moreover, R_{Zk} is defined as $R_{Zk} \equiv R_Z(\pi)R_k$. Then, continuous π rotations of the two axes of Z and k are given by

$$R_{Zk} = \begin{pmatrix} -\cos 2\phi & -\sin 2\phi & 0 \\ -\sin 2\phi & \cos 2\phi & 0 \\ 0 & 0 & -1 \end{pmatrix}. \tag{A19}$$

If the direction cosines for R_{Zk} are expressed as $R_{Zk}(a_j^{e_1})$ and $R_{Zk}(a_k^{e_2})$, then

$$R_{Zk}(a_j^{e_1}) = \begin{pmatrix} -\cos\theta\cos\phi \\ -\cos\theta\sin\phi \\ \sin\theta \end{pmatrix} = -(a_j^{e_1}) \tag{A20}$$

$$R_{Zk}(a_j^{e_2}) = \begin{pmatrix} -\sin\phi \\ \cos\phi \\ 0 \end{pmatrix} = -(a_j^{e_2}) \tag{A21}$$

$$P_{2\omega}^{e_2} = R_{Zk}(a_i^{e_2})d_{ijk}R_{Zk}(a_j^{e_1})R_{Zk}(a_k^{e_2})E_\omega^{e_1}E_\omega^{e_2} = -a_i^{e_2}d_{ijk}a_j^{e_1}a_k^{e_2}E_\omega^{e_1}E_\omega^{e_2}$$

$$= -\frac{A}{2}\cos(2\psi). \tag{A22}$$

Since $P_{2\omega}$ for the first crystal is the same as in equation (A22), the positioning of the second crystal shown in figures 6(a) and (b) will decide the difference between the results of figures 7(a) and (b). As in the former case (b), figure 6(a) should be shown by the next equation.

$$|P_{2\omega}^{\text{total}}|^2 = \frac{A^2}{8}\{\cos(4\psi) + 2\cos(3\psi) + 2\cos\psi + 3\} \tag{A23}$$

where $\psi = 0$ represents the case in which the positions of the c-axes are opposite and the crystal's X-axis directions are different from each other, as shown in figure 6(a), and the maximum value becomes $|P_{2\omega}^{\text{total}}|^2 = A^2$.

References

[1] Samanta L K, Yanagawa T and Yamamoto Y 1990 *Opt. Commun.* **76** 250
[2] Jacco J C, Loiacono G M, Jaso M, Mizelland G and Greenberg B 1984 *J. Cryst. Growth* **70** 484
[3] Zumsteg F C, Bierlien J D and Gier T E 1976 *J. Appl. Phys.* **47** 4980
[4] Gettemy D J, Harker W C, Lindholm G and Barnes N P 1988 *IEEE J. Quantum Electron.* **QE-24** 2231
[5] Yao J Q and Fahlen T S 1984 *J. Appl. Phys.* **55** 65
[6] Byer R L, Choy M M, Herbst R L, Chemla D S and Feigelson R S 1974 *Appl. Phys. Lett.* **24** 65
[7] Liu Y S, Dentz D and Belt R 1984 *Opt. Lett.* **9** 76
[8] Kato K 1986 *IEEE J. Quantum Electron.* **QE-22** 1013
[9] Garmash V M, Ermakov G A, Pavlova N I and Tarasov A V 1986 *Sov. Tech. Phys. Lett.* **129** 505
[10] Baumert J C, Schellenberg F M, Lenth W, Risk W P and Bjorklund G C 1987 *Appl. Phys. Lett.* **51** 2192
[11] Kato K 1988 *IEEE J. Quantum Electron.* **QE-24** 3
[12] Fan T Y, Huang C E, Hu B Q, Eckardt R C, Fan Y X, Byer R L and Feigelson R S 1987 *Appl. Opt.* **26** 2390
[13] Mehendale S C and Gupta P K 1988 *Opt. Commun.* **68** 301
[14] Boyd G D and Kleinman D A 1968 *J. Appl. Phys.* **39** 3597
[15] Kuizenga D J 1972 *Appl. Phys. Lett.* **21** 570
[16] Boyd G D, Ashkin A, Dziedzic J M and Kleinman D A 1965 *Phys. Rev.* A **137** 1305
[17] Volosov V D 1970 *Sov. Phys. Tech. Phys.* **14** 1652
[18] Miller R C, Boyd G D and Savage A 1965 *Appl. Phys. Lett.* **6** 77
[19] Shen Y R 1977 *Non-linear Infrared Generation* (Berlin: Springer) p 90
[20] Ashkin A, Boyd G D and Kleinman D A 1965 *Appl. Phys. Lett.* **6** 179
[21] Nikogosyan D N 1977 *Sov. J. Quantum Electron.* **QE-7** 1
[22] Ito H, Naito H and Inaba H 1975 *J. Appl. Phys.* **46** 3992
[23] Imoto N and Saito S 1989 *Phys. Rev.* A **39** 675
[24] Shelby R M and Levenson M D 1987 *Opt. Commun.* **64** 553
[25] Slusher R E, Hollberg L W, Yurke B, Mertz J C and Valley J F 1985 *Phys. Rev. Lett.* **55** 2409
[26] Wu L A, Kimble H J, Hall J L and Wu H 1986 *Phys. Rev. Lett.* **57** 2520